general Pol II transcription factors[7,20,25,26]. All protein fractions were dialysed against buffer B (25 mM Tris-HCl, pH 7.9, 50 mM KCl, 0.5 mM dithiothreitol, 0.1 mM EDTA and 20% glycerol (v/v)). 25-μl reactions contained either 25 ng 17M/5pAL7 and pG1 (ref. 5) or 100 ng pTEF(Δ-138) or pTEF(Δ-138_{TATA})[15], with aliquots of TFTC, TFIIDβ and recombinant TBP[5]. Where indicated, 200 ng purified anti-TBP monoclonal antibody 1C2 was also included in the reactions before the other factors were added. GAL-VP16-activated transcription was performed as described[5]. After the preincubation steps (30 min), transcription was initiated by addition of nucleoside triphosphates to 0.5 mM and $MgCl_2$ to 5 mM. Transcriptions were incubated at 25 °C for 45 min. Correctly initiated transcripts from the different promoters were analysed by quantitative S1 nuclease analysis[15,27].

DNase I footprinting. DNase I footprinting was performed as described[18,19]. The labelled AdMLP-containing probes were amplified by polymerase chain reaction on either the 17M5/pAL7 (ref. 28) (Fig. 3a) or the pM677 (ref. 29) (Fig. 3b) templates. For the footprinting experiments, ten times more TBP, TFIIDβ, and TFTC was used than in the transcription reactions.

Received 4 December 1997; accepted 6 March 1998.

1. Zawel, L. & Reinberg, D. Common themes in assembly and function of eukaryotic transcription complexes. *Annu. Rev. Biochem.* **64,** 533–561 (1995).
2. Roeder, R. G. The role of general initiation factors in transcription by RNA polymerase II. *Trends Biochem. Sci.* **21,** 327–335 (1996).
3. Verrijzer, C. P. & Tjian, R. TAFs mediate transcriptional activation and promoter selectivity [see comments]. *Trends Biochem. Sci.* **21,** 338–342 (1996).
4. Chang, M. & Jaehning, J. A. A multiplicity of mediators: alternative forms of transcription complexes communicate with transcriptional regulators. *Nucleic Acids Res.* **25,** 4861–4865 (1997).
5. Brou, C. *et al.* Distinct TFIID complexes mediate the effect of different transcriptional activators. *EMBO J.* **12,** 489–499 (1993).
6. Jacq, X. *et al.* Human TAFII30 is present in a distinct TFIID complex and is required for transcriptional activation by the estrogen receptor. *Cell* **79,** 107–117 (1994).
7. Bertolotti, A., Lutz, Y., Heard, D. J., Chambon, P. & Tora, L. hTAFII68 a novel RNA/SSDNA-binding protein with homology to the pro-oncoproteins TLS/FUS and EWS is associated with both TFIID and RNA polymerase II. *EMBO J.* **15,** 5022–5031 (1996).
8. Mengus, G. *et al.* Cloning and characterization of hTAFII118, hTAFII20 and hTAFII28; three subunits of the human transcription factor TFIID. *EMBO J.* **14,** 1520–1531 (1995).
9. Lescure, A. *et al.* The N-terminal domain of human TATA-binding protein plays a role in transcription from TATA-containing RNA polymerase II and III promoters. *EMBO J.* **13,** 1166–1175 (1994).
10. Usheva, A. & Shenk, T. TATA-binding protein-independent initiation: YY1, TFIIB, and RNA polymerase II direct basal transcription on supercoiled template DNA. *Cell* **76,** 1115–1121 (1994).
11. Timmers, H. T. M., Meyers, R. E. & Sharp, P. A. Composition of transcription factor B-TFIID. *Proc. Natl Acad. Sci. USA* **89,** 8140–8144 (1992).
12. Van der Knaap, J. A., Willem Borst, J., van der Vliet, P. C., Gentz, R. & Timmers, H. T. M. Cloning of the cDNA for the TATA-binding protein-associated $factor_{II}170$ subunit of transcription factor B-TFIID reveals homology to global transcription regulators in yeast and *Drosophila*. *Proc. Natl Acad. Sci. USA* **94,** 11827–11832 (1997).
13. Hansen, S. K., Takada, S., Jacobson, R. H., Lis, J. T. & Tjian, R. Transcription properties of a cell type specific TATA-binding protein, TRF. *Cell* **91,** 71–83 (1997).
14. Crowley, T. E., Hoey, T., Liu, J. K., Jan, Y. N., Jan, L. Y. & Tjian, R. A new factor related to TATA-binding protein has highly restricted expression patterns in *Drosophila*. *Nature* **361,** 557–561 (1993).
15. Boam, D. S., Davidson, I. & Chambon, P. A TATA-less promoter containing binding sites for ubiquitous transcription factors mediates cell type-specific regulation of the gene for transcription enhancer factor-1 (TEF-1). *J. Biol. Chem.* **270,** 487–494 (1995).
16. Nakajima, N., Horikoshi, M. & Roeder, R. G. Factors involved in specific transcription by mammalian RNA polymerase II: purification, genetic specificity, and TATA box-promoter interactions of TFIID. *Mol. Cell. Biol.* **8,** 4028–4040 (1988).
17. Pugh, B. F. & Tjian, R. Transcription from a TATA-less promoter requires a multisubunit TFIID complex. *Genes Dev.* **5,** 1935–1945 (1991).
18. Purnell, B. A., Emanuel, P. A. & Gilmour, D. S. TFIID sequence recognition of the initiator and sequences further downstream in *Drosophila* class II genes. *Genes Dev.* **8,** 830–842 (1994).
19. Oelgeschlager, T., Chiang, C. M. & Roder, R. G. Topology and reorganization of a human TFIID-promoter complex. *Nature* **382,** 735–738 (1996).
20. Dubrovskaya, V. *et al.* Distinct domains of $hTAF_{II}100$ are required for functional interaction with transcription factor TFIIFb (RAP30) and incorporation into the TFIID complex. *EMBO J.* **15,** 3702–3712 (1996).
21. Ruppert, S. & Tjian, R. Human TAFII250 interacts with RAP74: implications for RNA polymerase II initiation. *Genes Dev.* **9,** 2747–2755 (1995).
22. Hisatake, K. *et al.* Evolutionary conservation of human TATA-binding-polypeptide-associated factors TAFII31 and TAFII80 and interactions of TAFII80 with other TAFs and with general transcription factors. *Proc. Natl Acad. Sci. USA* **92,** 85–89 (1995).
23. Lavigne, A. C. *et al.* Multiple interactions between hTAFII55 and other TFIID subunits. Requirements for the formation of stable ternary complexes between hTAFII55 and the TATA-binding protein. *J. Biol. Chem.* **271,** 774–780 (1996).
24. Lennon, G., Auffray, C., Polymeropoulos, M. & Soares, M. B. The I.M.A.G.E. Consortium: an integrated molecular analysis of genomes and their expression. *Genomics.* **33,** 151–152 (1996).
25. Gerard, M. *et al.* Purification and interaction properties of the human RNA polymerase B(II) general transcription factor BTF2. *J. Biol. Chem.* **266,** 20940–20945 (1991).
26. De Jong, J. & Roeder, R. G. A single cDNA, hTFIIA/alpha, encodes both the p35 and p19 subunits of human TFIIA. *Genes Dev.* **7,** 2220–2234 (1993).
27. Tora, L. *et al.* The human estrogen receptor has two independent nonacidic transcriptional activation functions. *Cell* **59,** 477–487 (1989).
28. Brou, C. *et al.* Different TBP-associated factors are required for mediating the stimulation of transcription *in vitro* by the acidic transactivator GAL-VP16 and the two nonacidic activation functions of the estrogen receptor. *Nucleic Acids Res.* **21,** 5–12 (1993).
29. Moncollin, V., Miyamoto, N. G., Zheng, X. M. & Egly, J. M. Purification of a factor specific for the upstream element of the adenovirus-2 major late promoter. *EMBO J.* **5,** 2577–2584 (1986).

Acknowledgements. We thank P. Chambon for support; J. C. Dantonel for help in identification and cloning of hTLF; E. Scheer for technical assistance; Y. Lutz for antibodies; D. Boam, V. Dubrovskaya, A. C. Lavigne, G. Mengus, I. Davidson and the IMAGE Consortium for reagents; H. T. M. Timmers for antibodies and for discussing unpublished results; A. Bertolotti for discussions; D. J. Heard for discussions and reading the manuscript; P. Eberling for peptide synthesis; the cell culture group for HeLa cells; R. Buchert, J.-M. Lafontaine and B. Boulay for illustrations; and A. Özyhar for his contribution to the training of E.W. E.W. was supported by a fellowship from the Ministère de l'Enseignement Supérieur et de la Recherche. Research was supported by grants from the CNRS, the INSERM, the Hôpital Universitaire de Strasbourg, the Ministère de la Recherche et Technologie, the Fondation pour la Recherche Médicale and the Association pour la Recherche contre le Cancer.

Correspondence and requests for materials should be addressed to L.T. (e-mail: laszlo@titus.u-strasbg.fr).

corrections

Structure of the αβ tubulin dimer by electron crystallography

Eva Nogales, Sharon G. Wolf & Kenneth H. Downing

Nature **391,** 199–203 (1998)

In this Letter, the numbers for the secondary structure elements involved in Taxol binding are incorrect (page 202, second-to-last paragraph of main text). The sentences giving the correct numbers are, "In our model, the C-3′ is near the top of helix H1 (that is, between β:15–25), and the C2 group near H6 and the H6–H7 loop (that is, between β:212–222). The main interaction of the taxane ring is at L275, at the beginning of the B7–H9 loop." □

Spatial and temporal organization during cardiac fibrillation

Richard A. Gray, Arkady M. Pertsov & José Jalife

Nature **392,** 75–78 (1998)

The *x*-axis of Fig. 1d was mislabelled: the frequency values should instead read 0, 10, 20, 30, 40 Hz. □

Structure of the αβ tubulin dimer by electron crystallography

Eva Nogales, Sharon G. Wolf* & Kenneth H. Downing

Life Science Division, Lawrence Berkeley National Laboratory, Berkeley, California 94720, USA

The αβ tubulin heterodimer is the structural subunit of microtubules, which are cytoskeletal elements that are essential for intracellular transport and cell division in all eukaryotes. Each tubulin monomer binds a guanine nucleotide, which is non-exchangeable when it is bound in the α subunit, or N site, and exchangeable when bound in the β subunit, or E site. The α- and β-tubulins share 40% amino-acid sequence identity, both exist in several isotype forms, and both undergo a variety of post-translational modifications[1]. Limited sequence homology has been found with the proteins FtsZ[2] and Misato[3], which are involved in cell division in bacteria and *Drosophila*, respectively. Here we present an atomic model of the αβ tubulin dimer fitted to a 3.7-Å density map obtained by electron crystallography of zinc-induced tubulin sheets. The structures of α- and β-tubulin are basically identical: each monomer is formed by a core of two β-sheets surrounded by α-helices. The monomer structure is very compact, but can be divided into three functional domains: the amino-terminal domain containing the nucleotide-binding region, an intermediate domain containing the Taxol-binding site, and the carboxy-terminal domain, which probably constitutes the binding surface for motor proteins.

In the presence of zinc ions, purified tubulin assembles into two-dimensional sheets that are ideal samples for electron crystallography studies[4]. In these sheets, protofilaments appear to be similar to those in microtubules, but associated in an antiparallel fashion. The zinc-induced tubulin sheets used here are cold-labile and require GTP for assembly. Addition of taxol stabilizes the sheets against low-temperature depolymerization and ageing[4], an effect similar to that on microtubules. Taxol binds to a single site on the dimer in the sheets, near lateral contacts between protofilaments[5].

We have previously described three-dimensional density maps of tubulin at 6.5 and 4 Å (refs 5, 6). The present model has been built into a 3.7-Å map derived from a data set that includes 93 electron-diffraction patterns (providing structure factor amplitudes) and 159 images (providing experimental phases). Table 1 and Fig. 1 summarize the data. The high quality of the phases produced a clean map, with well defined connectivity, which is readily interpretable in terms of secondary-structure elements. The present model of tubulin has been built in the raw density map without refinement and includes all but the last 10 and 18 C-terminal residues of α- and β-tubulin, respectively. Figure 2 shows the density map and the model in several regions of the dimer.

The density maps for α- and β-tubulin are almost superimposable. Differences are limited to the length and conformation of some loops, very slight displacements (~1 Å) of some of the secondary-structure elements, and differences in side-chain densities. Owing to the similarity between monomers, our description and comments on the model apply to both α- and β-tubulin unless indicated otherwise. Residue numbers correspond to the aligned sequences of α- and β-tubulin as shown in Fig. 3, and include gaps in the sequence of β-tubulin.

Figure 4 shows the ribbon diagram of the tubulin dimer model (see later for 'dimer' definition). The core of the structure contains two β-sheets of 6 and 4 strands, flanked by 12 α-helices. Although there is no clear division of the density into domains in the map, it makes sense functionally to divide the structure of each monomer into three sequential domains.

The N-terminal domain includes residues 1–205 and forms a Rossmann fold, which is typical of nucleotide-binding proteins, in which parallel β-strands alternate with α-helices. Helices H1 and H2 are on one side of the sheet, whereas helices H3, H4 and H5 are on the other. Strands B2 and B3 are poorly defined in the unrefined density map. The residues in the loops connecting H1 and B2, and H2 and B3, are included for completeness, but were built in very weak density. These segments are long predicted loops on the putative inside surface of the microtubule, and correspond to a region of the sequence that can accommodate insertions and deletions[7].

Strand B6 leads to the intermediate domain, residues 206–381, containing a mixed β-sheet and five surrounding helices. The domain starts with helices H6 and H7, followed by a long loop and helix H8 at the longitudinal interface between monomers. B7 is a long β-strand that interacts with the β-sheet in the N-terminal domain. The loop connecting B7 and H9 is more ordered in α-tubulin, where it is involved in strong lateral contacts. Following a long loop

Table 1 Electron crystallographic data

Two-dimensional crystals	
Two-sided plane roup	$P12_1$
Unit cell	$a = 80, b = 92$ Å
Sampling thickness	$c = 90$ Å
Sample thickness	62 Å
Experimental data set	
Resolution cut-off	3.7 Å
Number of structure factors	12,000
Electron diffraction	
Number of patterns by tilt angle	18 (0°), 57 (45°), 19 (55°)
R_{sym}	19%
R_{merge}	25%
Image/phase data	
Number of images by tilt angle	12 (0°), 51 (45°), 86 (60°)
Phase residual by resolution zones	36° (5–4 Å), 46° (4–3.7 Å)

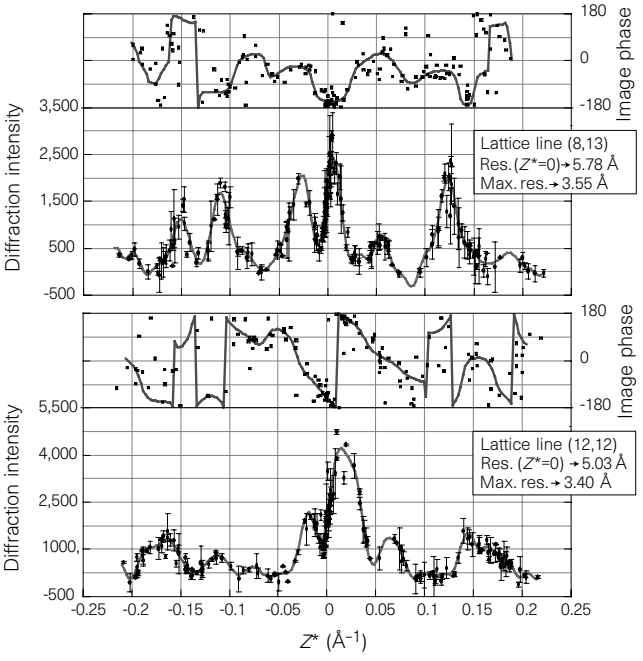

Figure 1 Experimental phase and intensity data and fitted curves for two representative reciprocal lattice lines. Error bars for the intensities are Friedel-pair differences. The resolution of each lattice line at the equator ($z^* = 0$) and its furthest point are indicated.

* Present address: Electron Microscopy Unit, Weizmann Institute of Science, Rehovot 76100, Israel.

come B8 and H10, which unravels at its C terminus in α-tubulin, followed by a very well defined short loop into B9. Finally, the loop between B9 and B10 includes an 8-residue insertion in the α-subunit which occludes the site that in β is occupied by taxol. The present model is compatible with the observation that C241 and C356 in the β-subunit can be crosslinked[8] (~8 Å apart in the model; Fig. 4b).

The C-terminal domain is formed by helices H11 and H12. These helices overlay the previous domains, sitting on the surface of the molecule that we have identified as the outside surface in the microtubule[9] (Fig. 4, legend). They are probably involved in the binding of MAPs and motor proteins. The loop connecting H11 and H12 is important for the interaction with the next monomer along the protofilament.

The last C-terminal residues of each monomer, missing from the model, correspond to the hypervariable part of the sequence where most of the differences between isotypes and across species occur. As the tubulin preparation we used included several α and β isotypes that are found in bovine brain, the inhomogeneity of the sample could contribute to the poor visibility in this part of the map. However, we do not see any significant difference in projection maps among αβIII, αβII, and undifferentiated tubulin (our unpublished results). This tubulin segment is highly acidic in both monomers and likely to be disordered, irrespective of the isotype composition.

The nucleotide in tubulin is positioned at the base of the Rossmann fold. The B1–H1, B2–H2 and B3–H3 loops, and the glycine-rich B4–H4 loop, appear to contact the phosphates. The

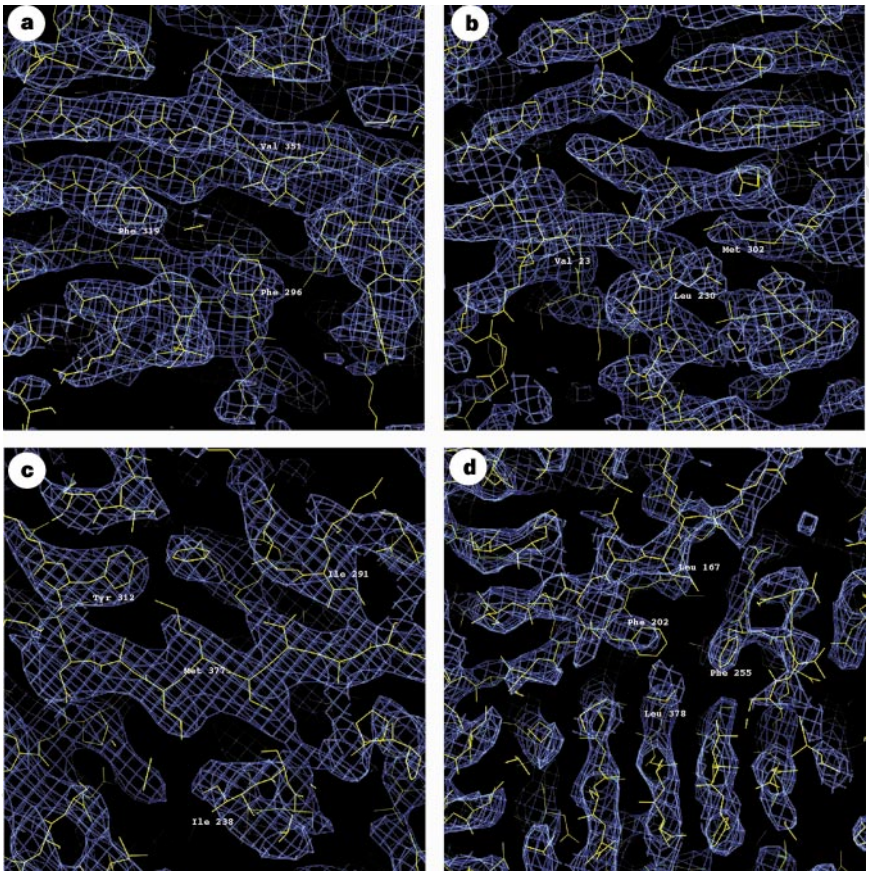

Figure 2 Sections of the experimental density map with the fitted model for different regions in the α- and β-tubulin molecules. **a**, **b**, Sections from β-tubulin; **c**, **d**, sections from α-tubulin. The map was calculated with a 3.7-Å cutoff. In the direction perpendicular to the crystals, the resolution is less than 3.7 Å, owing to the limit of 60° in tilt angle, but still sufficient that individual β-strands can be distinguished. The initial assignment of the sequence to the backbone trace was based mostly on the positions of aromatic side chains and on the connectivity of the density. Comparing corresponding densities in the α- and β-subunits, and relating the differences and similarities to those in their amino-acid sequences, were extremely helpful in tracing the chain. The sequence used for the model, in the absence of that from bovine brain tubulin, corresponds to porcine brain tubulin[28]. The numbering of residues is based on the alignment of the α- and β-tubulin sequences and so includes gaps in the sequence of β-tubulin (Fig. 3).

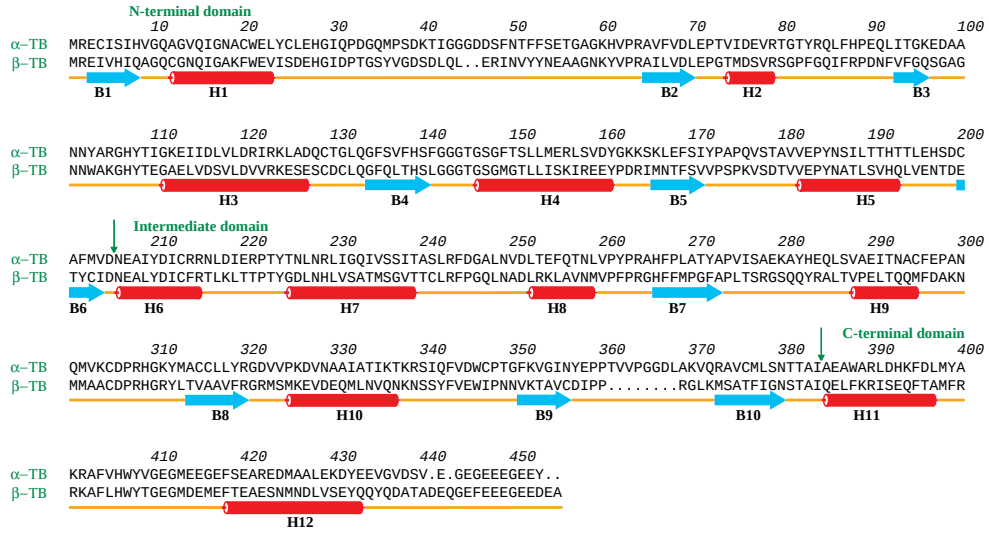

Figure 3 Sequences of pig brain α- and β-tubulin[28] used in the model (in the absence of tubulin sequences from cow we have used its closest known relative). Secondary structure elements are indicated and labelled as for Fig. 4. The tubulin preparations used in our experiments contained a mixture of isotypes. Most of the differences between isotypes are located at the extreme C terminus, which is not visible in our density. In most of the other positions of isotype differences, we arbitrarily chose the residue most similar to the other monomer.

B5–H5 loop is near the ribose, and N206 in H6, and Y224 and N228 in H7 interact with the nucleotide base. The position of the nucleotide agrees with models, based on comparison with other nucleotide-containing proteins, that position the phosphates near the glycine-rich loop. It is consistent with photocrosslinking experiments that locate C12 in β-tubulin near the guanine base[10], the peptide β157–176 near the ribose[11], and β65–79 by the γ-phosphate[12]. The position is also consistent with mutations in the region β105–111 affecting the hydrolysis of GTP[13]. Finally, C12 and either C203 or C213 can be crosslinked in β-tubulin, but only in the absence of the nucleotide[14]. In our model, the nucleotide is between those residues, but the distances between the cysteines are larger than 9 Å. However, the position of H6, containing C213, could easily be affected by the absence of nucleotide, bringing that cysteine closer to C12.

The nucleotide in one monomer interacts with the next monomer at the longitudinal interface. The interfaces between consecutive monomers in our density map are too similar to allow us to

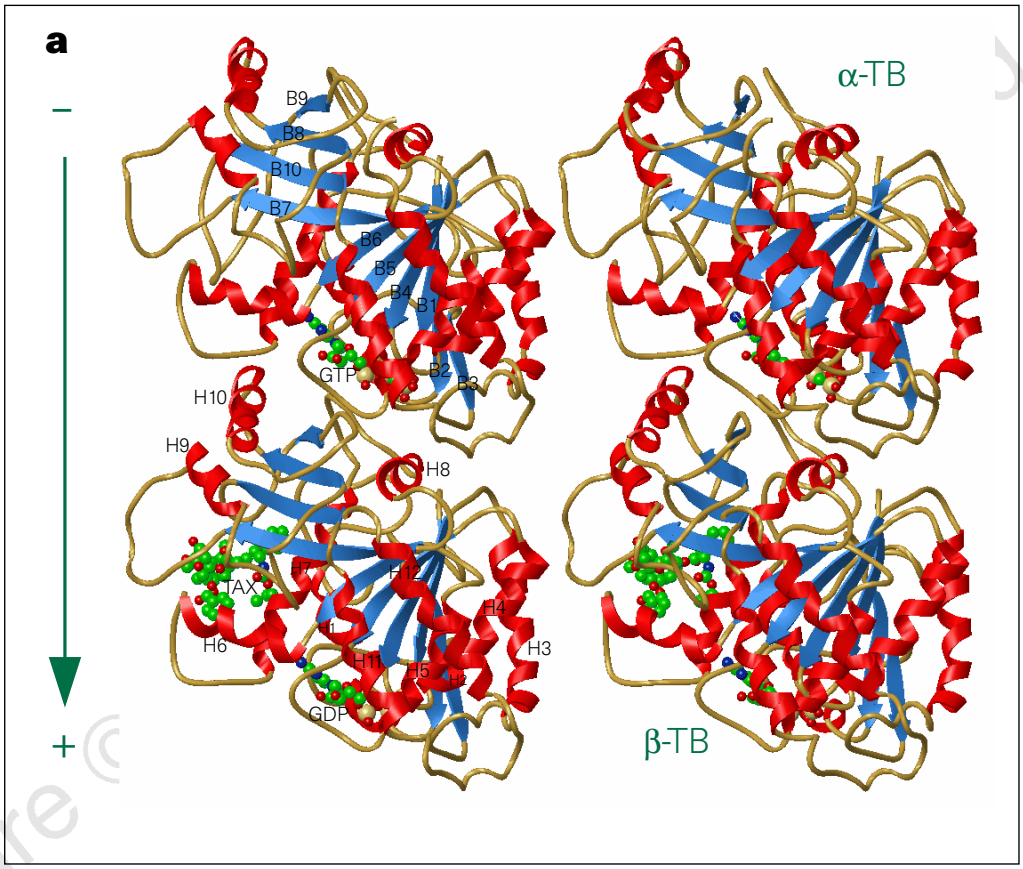

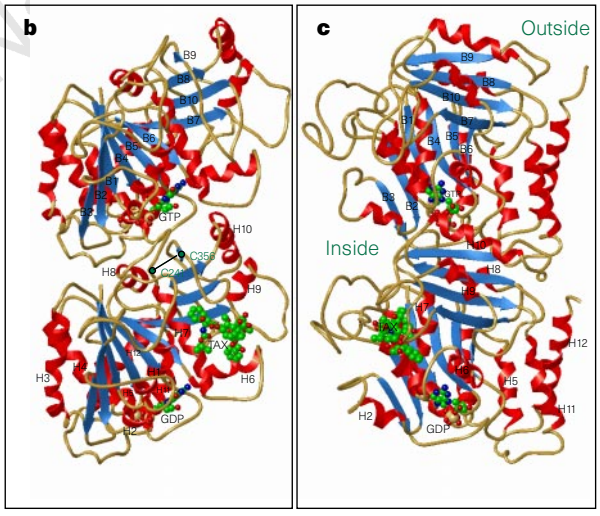

Figure 4 Ribbon diagram of the tubulin dimer showing α-tubulin with bound GTP (top), and β-tubulin containing GDP and taxotere (bottom). Labels for strands (in the α-subunit) and helices (in the β-subunit) are included. The arrow indicates the direction of the protofilament and microtubule axis. **a**, Stereo front view from the putative outside of the microtubule; **b**, back view from the putative inside of the microtubule; **c**, side view. Figures produced with AVS (Advanced Visual; ribbon module from M. Carson and A. Shah). The in–out orientation was determined by reference to reconstructions of intact microtubules[9]. Such reconstructions show prominent longitudinal ridge on the outside, which in our model would be formed by H11, H12 and the loop between H10 and B9, and shallow inside grooves giving the protofilament a bumpy appearance, corresponding in our model to H1, B3 and the long loops in the N-terminal domain. This represents the most likely arrangement of the dimer, because it buries the nucleotide that is at the non-exchangeable site in α (see text). For the nucleotide in β to be exchangeable at the plus end of a microtubule, the bottom of the figure would correspond to the plus end. We previously presumed the opposite orientation, based on a comparison of the zinc sheets in negatively stained, stain–glucose, and tannin–glucose embedding, with projection maps of open microtubules of known polarity in negative stain[9]. Some ambiguity in that determination may be introduced by uncertainty about the exact rotational alignment of the protofilament in the sheets with respect to those in open microtubules and by stain artefacts. The polarity with the plus end down would be consistent with experiments that located the β-subunit at the plus end of the microtubule[29] and the α-subunit at the minus end[30]. Circles in **b** indicate the positions of β Cys 241 and β Cys 356, separated by about 8 Å.

distinguish unequivocally between inter- and intradimer contacts (the interface near the N site is only slightly tighter than that by the E site). On the basis of the difference of exchangeability of nucleotide in the α and β monomers, we identified the intradimer interface as that in which the N site in the α-subunit is buried. The GTP at the E site in the β-subunit is partially exposed in the dimer but would be buried in the microtubule, where it becomes non-exchangeable. The assignment of the dimer shown in Fig. 4 thus provides the simplest explanation for nucleotide exchangeability in tubulin. Further support comes from data on the binding of colchicine. The main binding site of this drug is in the β-subunit, residues C356 and C241 (ref. 15) and region 1–36 (ref. 16) having been identified as part of the binding site (see the position of these residues in Fig. 4b). In addition, colchicine binds close to the αβ intradimer interface[17]. On the other hand, antibodies against β241–256, near the top of the β-monomer (Fig. 4b), and to α214–226, at the bottom of the α-monomer, bind to the dimer but are unable to bind to the microtubule[18]. An alternative dimer to that shown in Fig. 4 would more readily explain these results, although the present model would be compatible if changes in the dimer occurred on binding to the microtubule.

On the basis of the similar behaviour of our sheets and microtubules, we believe that hydrolysis at the E site occurs upon sheet polymerization. In agreement with this, we find extra density in α-tubulin that corresponds to the γ-phosphate. The similarity between the two monomers, in spite of their being in two different nucleotide-bound states, is not surprising. The current model is that the GDP-containing dimer buried in the microtubule is kept locked in a GTP-like conformation by the microtubule lattice, and that only upon depolymerization does the GDP dimer 'spring' into a different conformation[19]. Comparison by electron microscopy of microtubules formed in the presence of GTP or of non-hydrolysable GTP analogues have shown only a change of 1.5 Å in the axial repeat (less than 2% of the subunit length)[20,21].

The favoured polymers for tubulin-GDP are rings formed by curved protofilaments[22]. The conformation of tubulin-GDP is thus referred to as 'curved', as opposed to the 'straight' conformation of tubulin-GTP (or tubulin-GDP held locked in the microtubule lattice)[23]. In two simplified models, the curved conformation could either be one in which longitudinal contacts between dimers are at an angle (consistent with the dimer definition in Fig. 4), or one in which the dimer is bent at the monomer–monomer interface (alternative dimer definition). A more general model would involve extensive allosteric effects following hydrolysis, which could affect points distant from the nucleotide-binding pocket.

Our study was done on tubulin sheets that were stabilized by taxol. The model in Fig. 4 includes a molecule of taxotere, a Taxol analogue whose structure has been solved by X-ray crystallography[24] (in taxotere, the C-10 acetyl and the C-3′ benzamide groups of Taxol have been replaced respectively by a hydroxyl and a N-t-BOC group). In our map, there is clear density for the taxane ring, the most dense and least flexible part of Taxol. Some density is also clear for one of the side chains. The position in the model is based on the best visual fit to the observed density. This position is in good agreement with photocrosslinking results placing the C-3′ group near the sequence β: 1–31 (ref. 25), and the C2 group near the sequence β: 217–231 (ref. 26). In our model, the group at C-3′ is near the top of helix H1 (that is, between β: 15–25), and the C2 group near H5 and the H5–H6 loop (that is, between β: 212–222). The main interaction of the taxane ring with tubulin is at L275, at the beginning of the B8–H9 loop.

Our model of tubulin shows a compact molecular structure with three functional domains: namely, GTP-binding, drug-binding and motor/MAP-binding domains. The interaction between domains is very tight, so the effects that nucleotides, drugs and other proteins in the cell have on tubulin are firmly linked. The assembly of tubulin and its regulation through dynamic instability results from the fine tuning of the three components. Knowledge of the structure of tubulin should be invaluable for understanding the microtubule system in the cell.

The structure of the bacterial FtsZ protein is reported in this issue[27]. Comparison of the tubulin and FtsZ models indicates that they have a common structural core of identical fold, which includes 10 β-strands surrounded by 10 α-helices: more detail will be revealed by careful comparison of there two structures. □

Methods

Crystalline tubulin sheets were polymerized in the presence of zinc from bovine brain tubulin (Cytoskeleton Inc.) and stabilized with taxol as described[4]. Samples were prepared by tannin–glucose embedding and examined at liquid-nitrogen temperature in a JEOL 4000 electron microscope at 400 kV following previously described procedures[4,5]. Images were taken using spot-scan imaging and dynamic focus correction. Images and electron diffraction patterns were processed and merged as described[4,9].

Received 8 August; accepted 27 October 1997.

1. Ludveña, R. F. The multiple forms of tubulin: different gene products and covalent modifications. *Int. Rev. Cyt.* **178,** 207–275 (1998).
2. Mukherjee, A. & Lutkenhaus, J. Guanine nucleotide-dependent assembly of FtsZ into filaments. *J. Bacteriol.* **176,** 2754–2758 (1994).
3. Gabor Miklos, G. L., Yamamoto, M., Burns, R. G. & Maleszka, R. An essential cell division gene of *Drosophila*, absent from *Saccharomyces*, encodes an unusual protein with tubulin-like and myosin-like peptide motifs. *Proc. Natl Acad. Sci. USA* **94,** 5189–5194 (1997).
4. Nogales, E., Wolf, S.G., Zhang, S. X. & Downing, K. H. Preservation of 2-D crystals of tubulin for electron crystallography. *J. Struct. Biol.* **115,** 199–208 (1995).
5. Nogales, E., Wolf, S. G., Khan, I. A., Ludueña, R. F. & Downing, K. H. Structure of tubulin at 6.5 Å and location of the taxol-binding site. *Nature* **375,** 424–427 (1995).
6. Nogales, E., Wolf, S. G. & Downing, K. H. Visualizing the secondary structure of tubulin: three-dimensional map at 4 Å. *J. Struct. Biol.* **118,** 119–127 (1997).
7. Burns, R. G. & Surridge, C. D. in *Microtubules* (eds Hyams, J. S. & Lloyd, C. W.) 3–32 (Wiley, New York, 1993).
8. Little, M. & Ludueña, R. F. Structural differences between brain β1- and β2-tubulins: implications for microtubule assembly and colchicine binding. *EMBO J.* **4,** 51–56 (1985).
9. Wolf, S. G., Nogales, E., Kikkawa, M., Gratzinger, D., Hirokawa, N. & Downing, K. H. Interpreting a medium-resolution model of tubulin: comparison of zinc-sheet and microtubule structure. *J. Mol. Biol.* **263,** 485–501 (1996).
10. Shivanna, B. D., Mejillano, M. R., Williams, T. D. & Himes, R. H. Exchangeable GTP binding site of β-tubulin—identification of cysteine 12 as the major site of cross-linking by direct photoaffinity labeling. *J. Biol. Chem.* **268,** 127–132 (1993).
11. Hesse, J., Thierauf, M. & Ponstingl, H. Tubulin sequence region β155–174 is involved in binding exchangeable guanosine triphosphate. *J. Biol. Chem.* **262,** 15472–15475 (1987).
12. Linse, K. & Mandelkow, E.-M. The GTP-binding peptide of β-tubulin. Localization by direct photoaffinity labeling and comparison with nucleotide-binding proteins. *J. Biol. Chem.* **263,** 15205–15210 (1988).
13. Davis, A., Sage, C. R., Dougherty, C. A. & Farrell, K. W. Microtubule dynamics modulated by guanosine triphosphate hydrolysis activity of β-tubulin. *Science* **264,** 839–842 (1994).
14. Little, M. & Ludueña, R. F. Location of two cysteines in brain β_1-tubulin that can be cross-linked after removal of exchangeable GTP. *Biochim. Biophys. Acta* **912,** 28–33 (1987).
15. Bai, R. *et al.* Identification of cysteine 354 of β-tubulin as part of the binding site for the A ring of colchicine. *J. Biol. Chem.* **271,** 12639–12645 (1996).
16. Uppuluri, S., Knipling, L., Sackett, D. L. & Wolff, J. Localization of the colchicine-binding site of tubulin. *Proc. Natl Acad. Sci. USA* **90,** 11598–11602 (1993).
17. Shearwin, K. E. & Timasheff, S. N. Effect of colchicine analogs on the dissociation of αβ tubulin into subunits: the locus of colchicine binding. *Biochemistry* **33,** 894–901 (1994).
18. Andreu, J. M. Site-directed antibodies to tubulin. *Cell Motil. Cytoskel.* **26,** 1–6 (1993).
19. Caplow, M., Ruhlen, R. L. & Shanks, J. The free energy of hydrolysis of a microtubule-bound nucleoside triphosphate is near zero: all of the free energy for hydrolysis is stored in the microtubule lattice. *J. Cell Biol.* **127,** 779–788 (1994).
20. Vale, R. D., Coppin, C. M., Malik, F., Kull, F. J. & Milligan, R. A. Tubulin GTP hydrolysis influences the structure, mechanical properties, and kinesin-driven transport of microtubules. *J. Biol. Chem.* **269,** 23769–23775 (1994).
21. Hyman, A. A., Chrétien, D., Arnal, I. & Wade, R. H. Structural changes accompanying GTP hydrolysis of microtubules: information from a slowly hydrolyzable analog guanylyl-(α,β)-methylene-diphosphonate. *J. Cell Biol.* **128,** 117–125 (1995).
22. Díaz, J. F., Pantos, E., Bordas, J. & Andreu, J. M. Solution structure of GDP-tubulin double rings to 3 nm resolution and comparison with microtubules. *J. Mol. Biol.* **238,** 214–225 (1994).
23. Mandelkow, E. & Mandelkow, E.-M. Microtubules and microtubule-associated proteins. *Curr. Opin. Cell Biol.* **7,** 72–81 (1995).
24. Gueritte-Voegelein, F. *et al.* Structure of a synthetic taxol precursor: *N*-tert-butoxycarbonyl-10-deacetyl-*N*-debenzoyltaxol. *Acta Crystallogr. C* **46,** 781–784 (1990).
25. Rao, S., Krauss, N. E., Heerding, J. M., Orr, G. A. & Horwitz, S. B. 3′-(*p*-Azidobenzamido)taxol photolabels the N-terminal 31 amino acids of β-tubulin. *J. Biol. Chem.* **269,** 3132–3134 (1994).
26. Rao, S., Orr, G. A., Chaudhary, A. G., Kingston, D. G. I. & Horwitz, S. B. Characterization of the taxol binding site on the microtubule. *J. Biol. Chem.* **270,** 20235–20238 (1995).
27. Löwe, J. Y. & Amos, L. A. Crystal structure of the bacterial cell-division protein FtsZ complexed with GDP. *Nature* **391,** 203–206 (1998).
28. Ponstingl, H., Krauhs, E., Little, M., Kempf, T., Hofer-Warbinek, R. & Ade, W. Amino acid sequence of α- and β-tubulins from pig brain: heterogeneity and regional similarity to muscle proteins. *Cold Spring Harbor Symp. Quant. Biol.* **46,** 191–197 (1982).
29. Mitchison, T. J. Localization of an exchangeable GTP binding site at the plus end of microtubules. *Science* **261,** 1044–1047 (1993).

30. Fan, J., Griffiths, A. D., Lockhart, A., Cross, R. A. & Amos, L. A. Microtubule minus ends can be labeled with a phage display antibody specific to α-tubulin. *J. Mol. Biol.* **259,** 325–330 (1996).

Acknowledgements. We thank R. F. Ludueña for isotypically purified αβII and αβIII tubulin, M. Le for help with electron diffraction processing, and R. M. Glaeser and Y. L. Han for comments on the manuscript. Taxol was provided by the Drug Synthesis and Chemistry Branch, Division of Cancer Treatment of the National Cancer Institute. This work was supported by the NIH.

Correspondence and requests for materials should be addressed to E.N. Coordinates referred to in this Letter have been deposited in the Brookhaven Protein Data Bank with ID 1tub and will be accessible within one year.

Crystal structure of the bacterial cell-division protein FtsZ

Jan Löwe & Linda A. Amos

MRC Laboratory of Molecular Biology, Cambridge CB2 2QH, UK

Bacterial cell division ends with septation, the constriction of the cell wall and cell membranes that leads to the formation of two daughter cells[1,2]. During septation, FtsZ, a protein of relative molecular mass 40,000 which is ubiquitous in eubacteria and is also found in archaea and chloroplasts[3], localizes early at the division site to form a ring-shaped septum. This septum is required for the mechanochemical process of membrane constriction[4]. FtsZ is a GTPase[5,6] with weak sequence homology to tubulins[7]. The nature of FtsZ polymers *in vivo* is unknown, but FtsZ can form tubules, sheets and minirings *in vitro*[8,9]. Here we report the crystal structure at 2.8 Å resolution of recombinant FtsZ from the hyperthermophilic methanogen *Methanococcus jannaschii*. FtsZ has two domains, one of which is a GTPase domain with a fold related to one found in the proteins p21^{ras} and elongation factor EF-Tu. The carboxy-terminal domain, whose function is unknown, is a four-stranded β-sheet tilted by 90° against the β-sheet of the GTPase domain. The two domains are arranged around a central helix. GDP binding is different from that typically found in GTPases and involves four phosphate-binding loops and a sugar-binding loop in the first domain, with guanine being recognized by residues in the central connecting helix. The three-dimensional structure of FtsZ is similar to the structure of α- and β-tubulin[10].

Two FtsZ genes (named after filamenting temperature-sensitive mutant Z) from the archaeon *M. jannaschii* have been characterized by the genome project[11]. One gene, MJ0370, was amplified by genomic polymerase chain reaction (PCR) and expressed in *E. coli*/C41, a mutant of BL21 capable of expressing toxic genes[12]. Proteolysis during cell disruption was minimized by using heat-shock treatment. Cubic crystals were obtained and the structure was solved by multiple isomorphous replacement and density modification (see Methods and Table 1). The model (Fig. 1) contains residues 23–356, 116 water molecules, and one molecule of GDP; weak density for residues 1–22 was visible as an extension from helix H0.

FtsZ consists of two domains with a long, 23-residue, helix H5 (Figs 1a, 2) connecting them. The N-terminal portion of the molecule, containing residues 38–227, has GDP obtained from the expression host bound to it and will be called the GTPase domain. It consists of a six-stranded parallel β-sheet surrounded by two and three helices on both sides. The overall fold of the GTPase domain of FtsZ is related to typical GTPases and can be superimposed on the p21^{ras}–GDP complex (Protein Data Bank (PDB) entry 1Q21; ref. 13) using 52 Cα atoms (S1, H1, S2, H2, S4, H3 and S5) to give a root-mean-squared (r.m.s.) deviation of 1.88 Å. The topology of the β-sheet in FtsZ is 321456, which is slightly different from the topology in p21^{ras} (ref. 13), where it is 231456, but, together with the arrangement of five helices (H1, HL1, H2, H3 and H4), is consistent with typical Rossmann-fold topology[14]. Helix H2A is unique to FtsZ. Numbering of secondary structure elements (Fig. 2) follows the corresponding elements of p21^{ras} proteins.

The C-terminal domain, spanning residues 228–356, consists of a mainly parallel four-stranded central β-sheet supported by two helices on one side. The topology of the sheet is 1423, with strand 4 antiparallel to the others. The uncovered side of the sheet makes contacts with helix H5 and is otherwise open to the solvent. The fold of the C-terminal domain is related to chorismate mutase of *Bacillus subtilis* and can be superimposed on PDB entry 1COM[15] with an r.m.s. deviation of 1.83 Å over 52 Cα atoms (SC1, HC2, SC2, HC3, SC3 and SC4). Additionally, sequence comparisons give similarities to calmodulins in three loop regions (Swissprot CALM-TRYCR; loops between H5/HC1, SC1/HC2, and SC2/HC3) and to adenylyl cyclase (CYA1_HUMAN; residues 620–740), making a role in calcium binding feasible. The electrostatic potential on the

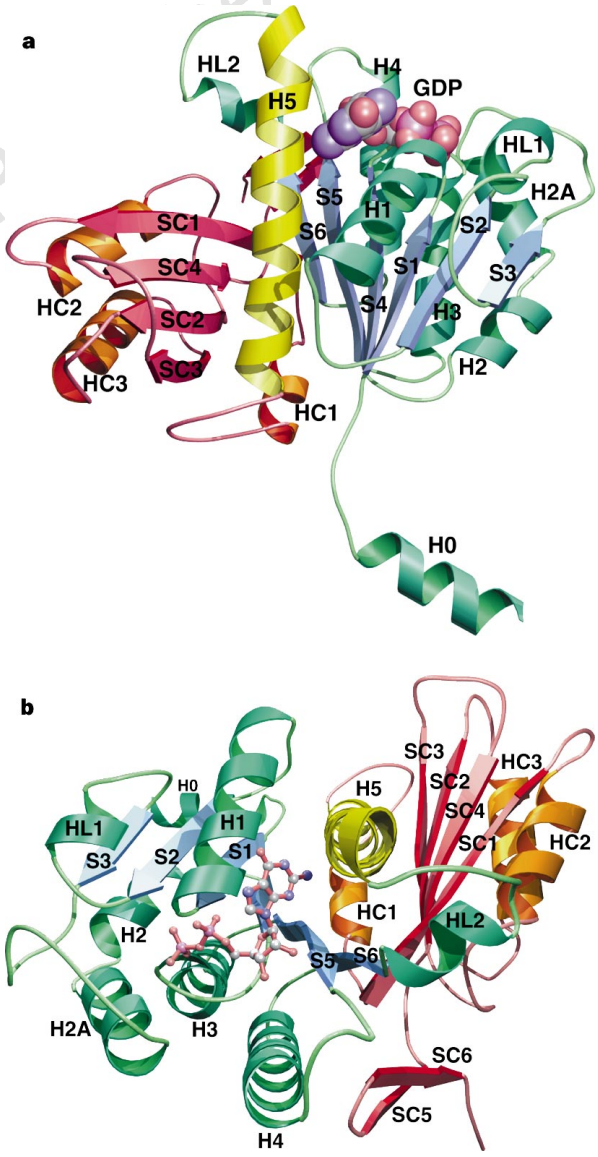

Figure 1 Ribbon drawings of FtsZ (residues 23–356) from *M. jannaschii*. **a**, View showing the GTPase domain in blue/green, the C-terminal domain in red/orange, and the connecting helix H5 in yellow. GDP is represented by a space-filling model. **b**, View of FtsZ rotated by ~90° from that in **a**. GDP is represented by a ball-and-stick model. Figures were prepared with POVSCRIPT (D. Peisach, personal communication)[28].